Supplement of Atmos. Meas. Tech., 9, 3969–3986, 2016
http://www.atmos-meas-tech.net/9/3969/2016/
doi:10.5194/amt-9-3969-2016-supplement

Atmospheric Measurement Techniques
Open Access
EGU

Supplement of

Clustering, methodology, and mechanistic insights into acetate chemical ionization using high-resolution time-of-flight mass spectrometry

Patrick Brophy and Delphine K. Farmer

Correspondence to: Patrick Brophy (pbrophy@colostate.edu) and Delphine K. Farmer (delphine.farmer@colostate.edu)

SI 1: Experimental Setup

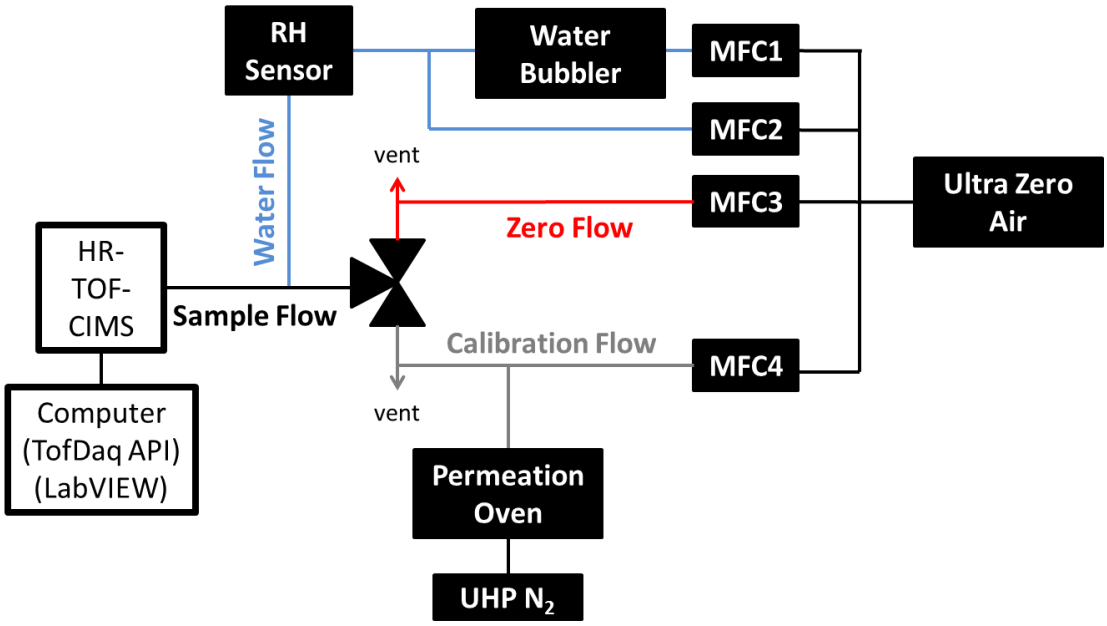

Figure SI1: Schematic diagram of the automated experimental setup for used calibrating the HR-TOF-CIMS under different voltage and humidity conditions. All tubing leading from ultra zero air source to MFCs was 1/8'' stainless steel tubing. Tubing from the N_2 source to the permeation oven is also 1/8'' stainless steel. The tubing on the zero air flow is stainless steel to ensure purity of zero air. All tubing wetted with calibration compounds is ¼'' PFA (i.e. calibration flow and sample flow). The tubing used for the water flows are all ¼'' PFA once water is present in the line and stainless steel where only ultra zero air is present. The calibration flows range from 1-20 SLPM. Zero flows are set such that the vent is always flowing (<2 SLPM). The water flow is set such that the sample flow subsamples the calibration flow and zero flow at flow rates >100 sccm. The total flow into the HR-TOF-CIMS is ~2 SLPM.

SI 2: Thuner determined voltage configuration starting point

Table SI1 Initial Voltage Configuration (Thuner Derived)	
Component	Voltage (V)
IMR Vacuum Region (100 mbar) SH-112 Agilent Single Scroll Pump	
IMR	-22
Short Segmented Quadrupole Region (2 mbar) Agilent TriScroll 600	
Nozzle	1.768
SSQ Entrance Plate	-2.766
SSQ Front	6.492
SSQ Back	4.196
Lens Skimmer	5.303
Skimmer	12
Big Segmented Quadrupole Region (1.3×10^{-3} mbar) Split Flow Pfeiffer Turbo Pump Stage 1	
BSQ Front	13
BSQ Back	13
Skimmer	20.194
Primary Beam Region (1.12×10^{-4} mbar) Split Flow Pfeiffer Turbo Pump Stage 2	
Ref. (Bias)	56.617
Ion Lens	91.604
Deflector Flange	91.35
Deflector	95.25
Time-of-Flight Region (7.5×10^{-7} mbar) Split Flow Pfeiffer Turbo Pump Stage 3	
TOF Pulse	700
TOF Reference	43.895
TOF Extraction 1	30
TOF Extraction 2	700
TOF Lens	0
Drift	3000
Reflectron Grid	645.247
Reflectron Back	700
Post Acceleration	2800

SI 2.1: Thuner Method General Setup

The HR-TOF-CIMS continuously samples Ultra Zero Grade Air (Airgas, Inc.) to maintain stable signal across the mass range used for the Thuner experiments. Two zero air systems were also investigated (Environics, Inc. and Aadco Instruments, Inc.), but these systems cause instabilities and are not suitable for long Thuner experiments (or most CIMS work in general). The set of voltages chosen to create all subsequent voltage configurations are shown in Table SI1.

The approach to these Thuner experiments is to control clustering while optimizing the voltage configurations to maximize ion transmission efficiency. All of the controlling factors are summarized in Table SI2. All of the ions used for responses are summarized in Table SI3. The summary of results is presented in Figure SI2. Cluster control is primarily accomplished by controlling the voltage difference between the BSQ front and last skimmer in the SSQ (component relation 5) because this set of components is most sensitive towards controlling cluster transmission. The ions used to track sensitivity are all deprotonated-declustered ions. The idea is that cluster transmission is essentially held constant at each tuning step by constraining the system at component relation 5. Then the absolute ion transmission efficiency can be improved by monitoring the chosen ions. This is not exactly correct because other components can float to high or low voltage differences leading to more or less declustered operation; this can be overcome by more constrained control over the various API component relations. This effect is practically dealt with by simply post-processing the Thuner results and using the ratio between the signal of the [acetate + acetic acid] cluster and the acetate ion as the filtering criteria for choosing the voltage files.

Figure S1 (top) shows all the voltage experiments for the complete Thuner experiment. Each step is repeated 10 times with small allowable voltage ranges applied to each component. This allows Thuner to test voltage sets within a fairly small voltage space where optimizations are better constrained. The skimmer to BSQ voltage difference is changed after tuning the SSQ, BSQ, and TOF voltages using a single voltage range. Seven voltage ranges are used (0-3 V, 4-6 V, 7-9 V, 10-12 V, 13-15 V, 16-18 V, and 19-21 V).

The observed decrease in average ion signal at high clustering ratios arises from the choice of response ions being deprotonated-declustered ions. Much less acetate makes it through the API because a large fraction of the acetate ion is bound up in clustering reactions. This can be seen in the Figure SI1 (bottom panel) specifically examining the [acetate + acetic acid] cluster and acetate. At low voltage differences (high acetate cluster ratio) there is a huge signal from [acetate + acetic acid] cluster which rapidly decreases as a function of voltage difference. The opposite trend is true for acetate.

These considerations highlight the difficulty of tuning the API with Thuner. Two possible approaches exist for future investigations: highly constrained tuning and highly targeted tuning. This manuscript (main paper) shows that the various components in the API have knowable relationships, and their effects are only observed under certain voltage differences. Thus, it seems possible to tune while keeping all these voltage differences within certain ranges that will not significantly contribute to either relative ion transmission effects (e.g. voltage differences across the quadrupoles) or declustering effects. Then a single component relationship (skimmer to BSQ front) may be used to control clustering. The other, and probably simpler option, is to let Thuner to the work by targeting certain performance criteria. Acetate, formate, and chloride are used as response variables in the work discussed here.

Alternatively, one could define the acetate cluster ratio and use this number as a specific target. Key components can still be constrained using this targeted mode of tuning.

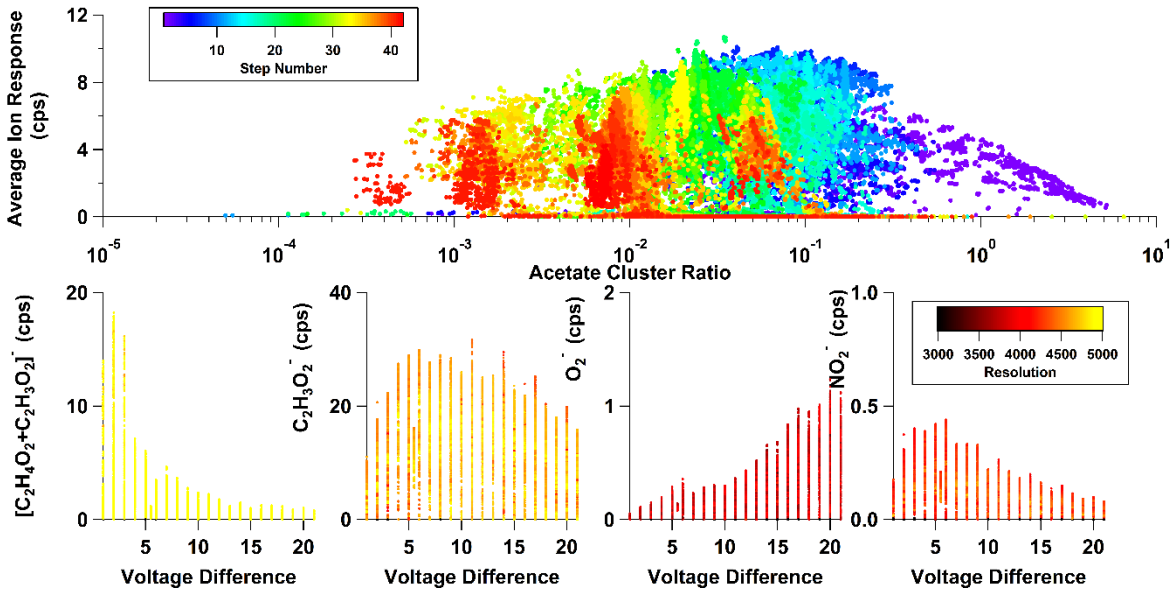

Figure SI2: Thuner results of various ions and average response. Each point is one voltage configuration. Top: the average ion response is colored by the Thuner step number and plotted as a function of the acetate cluster ratio. Bottom: The average ion response of individual species is plotted as a function of applied voltage difference between the last skimmer of the SSQ vacuum region and the BSQ entrance. These data are colored by the resolution of the detected peak.

Table SI2
Thuner API Voltage Relations

Relationship Name	Components	Vacuum Region	Comments
Step 1: SSQ Tuning Step			
IMR	IMR	IMR	
Nozzle	Nozzle	IMR to SSQ	
SSQ Entrance Plate	SSQ Entrance Plate	SSQ	
SSQ Average	(SSQ front + SSQ Back)/2	SSQ	Average voltage of SSQ
SSQ Difference	SSQ Back – SSQ Front	SSQ	Voltage drop across SSQ
Lens Skimmer	Lens Skimmer	SSQ	
SSQ-BSQ Transition	BSQ Front – Skimmer	SSQ to BSQ	Voltage drop from last SSQ region skimmer to BSQ front
BSQ Average	(BSQ front + BSQ Back)/2	BSQ	Average voltage of BSQ
BSQ Difference	BSQ Back – BSQ Front	BSQ	Voltage drop across BSQ
Step 2: BSQ/PB Tuning Step			
Lens Skimmer	Lens Skimmer	SSQ	
SSQ-BSQ Transition	BSQ Front – Skimmer	SSQ-BSQ	Voltage drop from last SSQ region skimmer to BSQ front
BSQ Average	(BSQ front + BSQ Back)/2	BSQ	Average voltage of BSQ
BSQ Difference	BSQ Back – BSQ Front	BSQ	Voltage drop across BSQ
Skimmer 2	Skimmer 2	BSQ	
Reference	Reference	PB	
Deflector Average	(deflector + deflector flange)/2	PB	Average voltage of lens stack
Deflector Difference	deflector flange – deflector	PB	Difference of lens stack
Lens	Lens	TOF	
Step 3: PB/TOF Tuning			
Reference	Reference	PB	
Deflector Average	(deflector + deflector flange)/2	PB	Average voltage of lens stack
Deflector Difference	deflector flange – deflector	PB	Difference of lens stack
Lens	Lens	TOF	
TOF Extraction Pulse 1	TOF Extraction Pulse 1	TOF	
TOF Extraction Reference	TOF Extraction Reference	TOF	
Reflectron Grid	Reflectron Grid	TOF	

Table SI3 Thuner Ions		
All Tuning Steps		
Ion	Used for m/z calibration	Used for sensitivity response
O_2^-	Yes	No
Cl^-	Yes	Yes
CHO_2^-	Yes	Yes
NO_2^-	Yes	No
$CH_3CO_2^-$ (Acetate Reagent Ion)	Yes	Yes
NO_3^-	Yes	No
$C_4H_7O_4^-$ (Acetate Reagent Cluster)	Yes	No

SI 3: Proposed mechanism for observed [$\bullet C_2H_3O_5$ + Acetate]$^-$ cluster

Alpha-particle emission from ^{210}Po

$^{210}Po \rightarrow \alpha + {}^{206}Pb$ (SI R1)

$\alpha + N_2 \rightarrow \alpha + N_2^+ + e^-$ (SI R2)

Electron capture and dissociation of Acetic Anhydride

$H_3CC(O)O(O)CCH_3 + e^- \rightarrow H_3CC(O)O(O)CCH_3^-$ (SI R3)

$H_3CC(O)O(O)CCH_3^- + M \rightarrow H_3CC(O)O^- + \bullet(O)CCH_3^-$ (SI R4)

Auto-oxidation of radical fragment

$\bullet(O)CCH_3^- + 2O_2 \rightarrow \bullet C_2H_3O_5$ (SI R5)

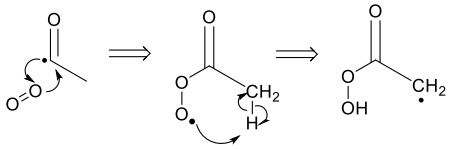

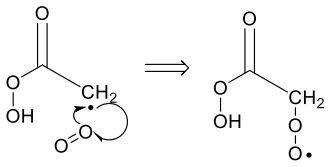

Cluster Formation of Radical

$CH_3C(O)O^- + \bullet C_2H_3O_5 \rightarrow [CH_3C(O)O + \bullet C_2H_3O_5]^-$ (SI R6)

SI 4: Effect of [acetic anhydride] on observed background spectra and reagent ions

Bertram *et al.* (2011) show a mass spectrum with an [acetate + acetic acid]/acetate ratio of 5.54 and an [acetate + 2(acetic acid)]/acetate ratio of 0.83. Both of these clusters are in much higher abundance in that study than has ever been observed on our instrument. Additionally, the peak at m/z 166 corresponds to $[CH_3C(O)O^- + \bullet C_2H_3O_5]^-$ in our system. This peak is observed by Bertram *et al.* (2011), but is very small compared to the [acetate + 2(acetic acid)] cluster. Thus, API tuning alone probably does not explain the differences observed between our instruments because one would assume that the $[CH_3C(O)O^- + \bullet C_2H_3O_5]^-$ cluster would be transmitted easily given the abundance of the higher order cluster.

The amount of acetic anhydride added to these systems remains a difficult number to constrain because liquid filled reservoirs are routinely used to generate acetate reagent ions. We attempted heating and cooling experiments that show subtle changes in the abundance and ratio of the dominate species produced from acetate CIMS. Figure SI3 shows the experimental results. Briefly, the acetic anhydride glass reservoir, stainless steel transfer lines, and Po-210 ionizer are constantly heated using heating rope and a PID temperature controller during normal operation. This entire heating system is turned off during this experiment and allowed to cool while the HR-TOF-CIMS continues acquiring mass spectra. This experiment is conducted under two voltage configurations (high declustering mode dV=20 and cluster mode dV=2) and two relative humidity settings (0% and 80% RH).

No change is observed under declustered settings further highlighting the importance of running this instrument in cluster mode to understand the underlying ion-neutral chemistry occurring in the IMR. Operation under cluster mode shows significant changes. Under dry conditions, the [acetate + 2(acetic acid)] cluster and the [acetate + water] cluster are observable but very small. Increasing the temperature (more acetic anhydride) leads to an increase in both the [acetate + acetic acid] and [acetate + 2(acetic acid)] clusters while slightly decreasing the $[CH_3C(O)O^- + \bullet C_2H_3O_5]$ cluster. Under high relative humidity conditions, the [acetate + 2(acetic acid)] is very small and barely detectable. The [acetate + water] and $[CH_3C(O)O^- + \bullet C_2H_3O_5]$ clusters decreases as more acetic anhydride is added to the Po-210 ionizer. It is not expected that adding huge amounts of acetic anhydride will ever be sufficient to titrate out the [acetate+water] cluster because it makes up a very large fraction of the total signal.

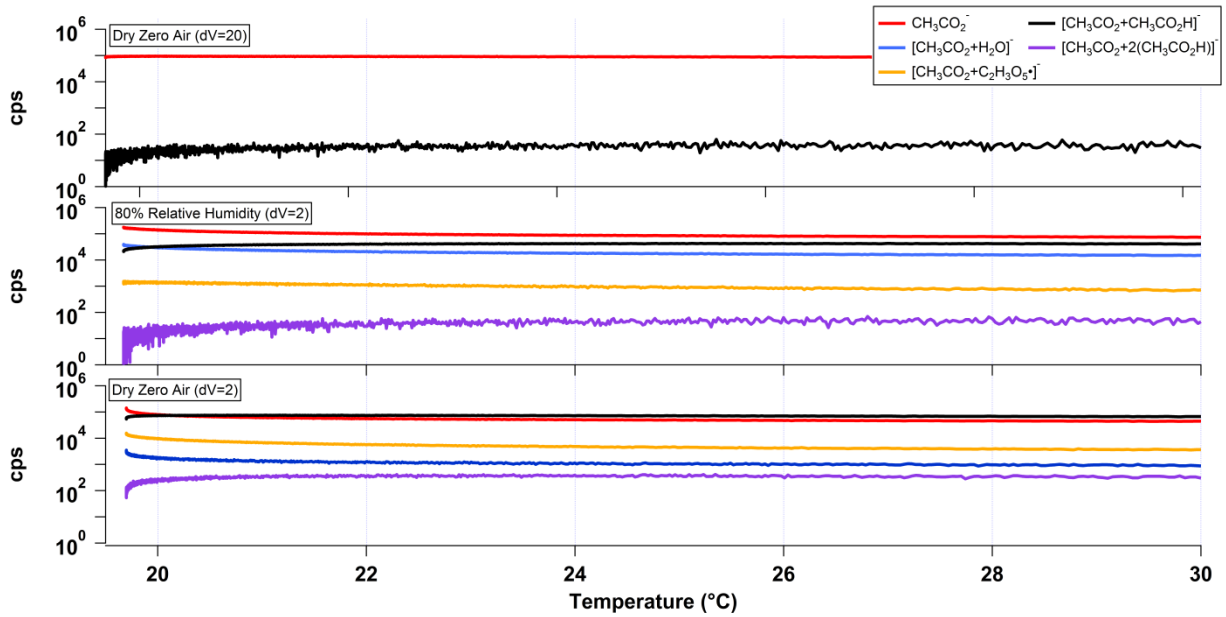

Figure SI3: The effect of heating and cooling the acetic anhydride reservoir and transfer lines on the observed reagent ion signals. The heating/cooling cycle is conducted under declustered settings (top) and clustered settings (middle and bottom). Relative humidity is set to 80% under cluster mode (middle) for comparison to dry experiments under cluster mode (bottom).

SI 5: Other calibrations and additional data

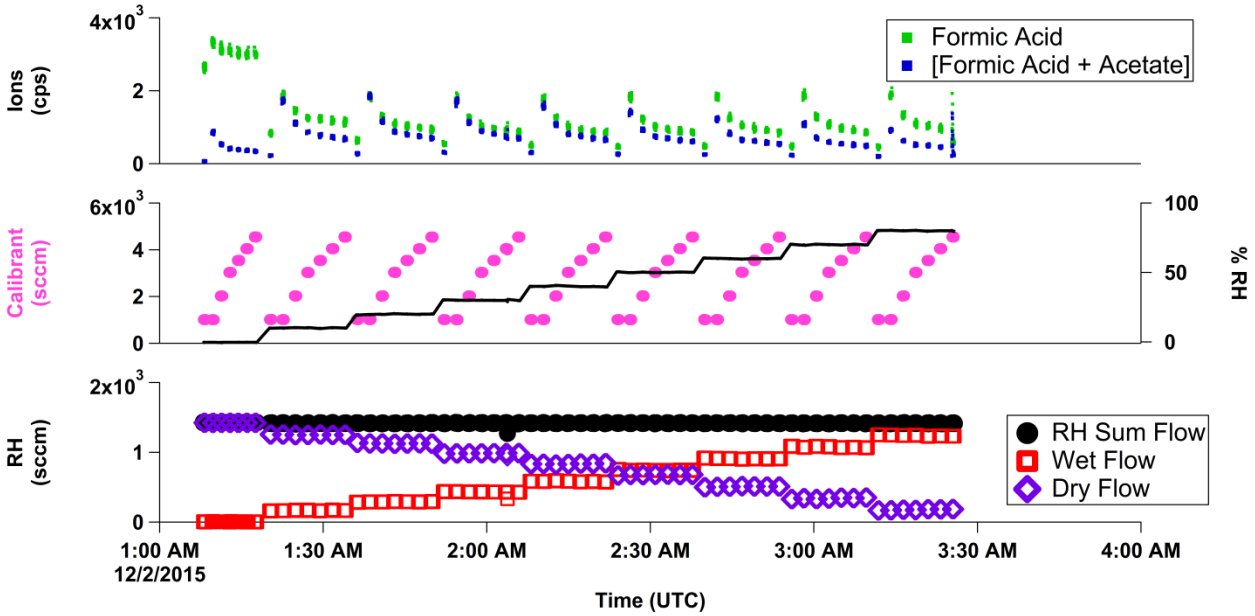

Figure SI4: Detailed summary of experimental calibration procedure for voltage and relative humidity dependent calibrations. (Bottom) Relative humidity control system: the flow from the MFC pushing ultra zero air through a series of water filled glass bubblers and the flow from the MFC controlling the dry air flow. The sum of these two controllers is held constant. (Middle) The resulting relative humidity generated from the relative humidity control system measured from the inline relative humidity sensor is plotted on the right axis. The MFC controlling the dilution flow of the calibration source is plotted on the left axis. (Top) The ion signal is shown for formic acid and the [acetate + formic acid] cluster during the calibration experiment.

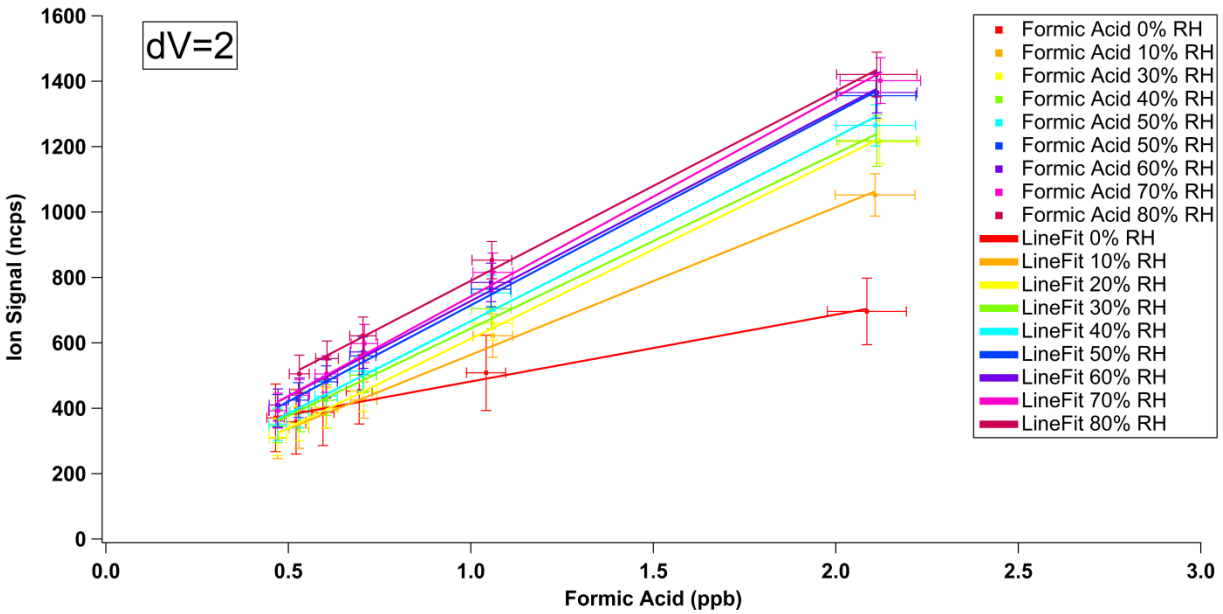

Figure SI5: Normalized and background subtracted calibration curves colored by relative humidity and collected under a single voltage configuration using the experimental setup graphically described in Figure SI3. These data are automatically generated for all species investigated. Deprotonated-declustered formic acid is shown here.

SI 5.1 Sensitivity

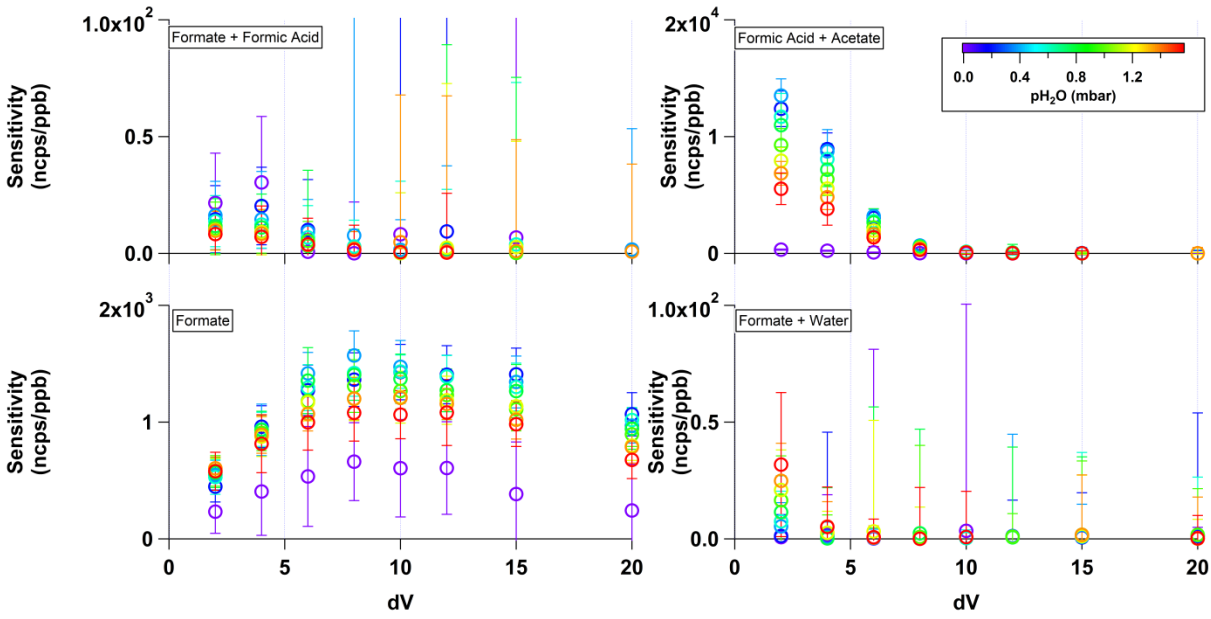

Figure SI6: The sensitivity to formic acid and related clusters is plotted against the voltage difference applied between the skimmer and BSQ front (component relation 5). The points are colored by the calculated partial pressure of water in the IMR corresponding to changing the relative humidity from 0% to 80% under laboratory conditions. Sensitivity drops off at higher dV values for clustered species but is maintained for declustered-deprotonated ions.

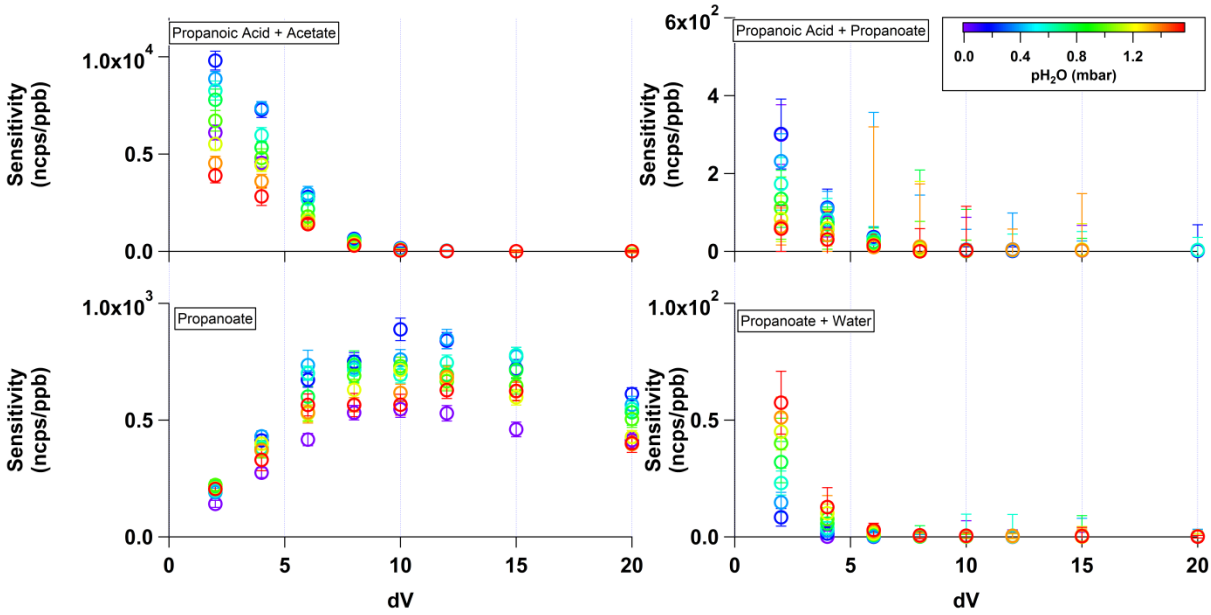

Figure SI7: The sensitivity to propanoic acid and related clusters is plotted against the voltage difference applied between the skimmer and BSQ front (component relation 5). The points are colored by the calculated partial pressure of water in the IMR corresponding to changing the relative humidity from 0% to 80% under laboratory conditions. Sensitivity drops off at higher dV values for clustered species but is maintained for declustered-deprotonated ions.

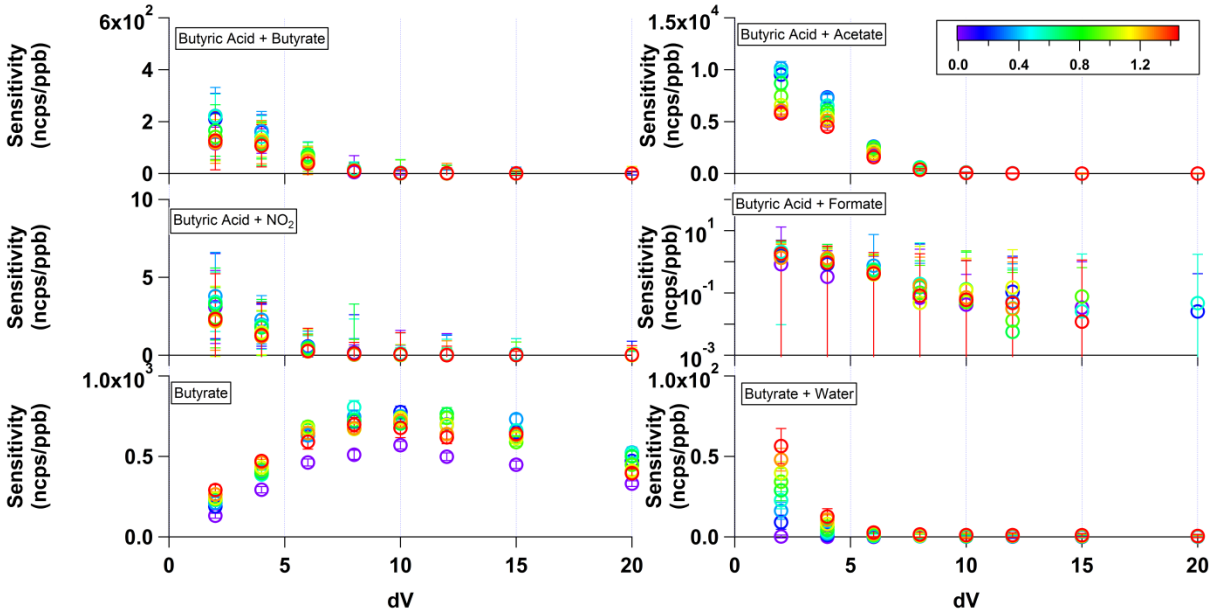

Figure SI8: The sensitivity to butyric acid and related clusters is plotted against the voltage difference applied between the skimmer and BSQ front (component relation 5). The points are colored by the calculated partial pressure of water in the IMR corresponding to changing the relative humidity from 0% to 80% under laboratory conditions. Sensitivity drops off at higher dV values for clustered species but is maintained for declustered-deprotonated ions.

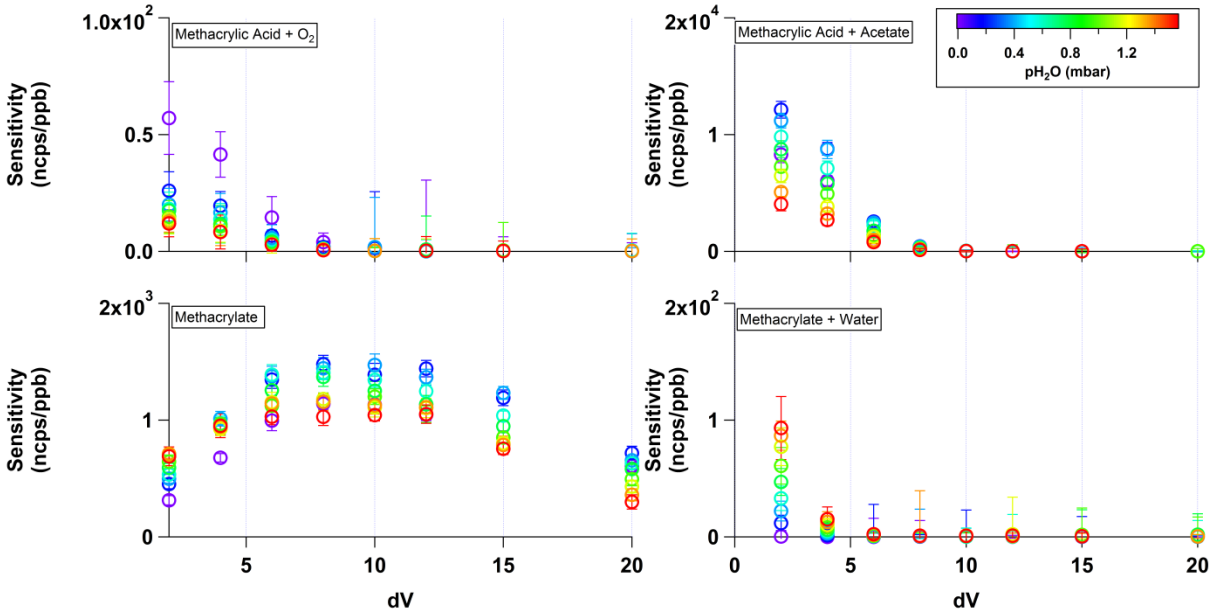

Figure SI9: The sensitivity to methacrylic acid and related clusters is plotted against the voltage difference applied between the skimmer and BSQ front (component relation 5). The points are colored by the calculated partial pressure of water in the IMR corresponding to changing the relative humidity from 0% to 80% under laboratory conditions. Sensitivity drops off at higher dV values for clustered species but is maintained for declustered-deprotonated ions.

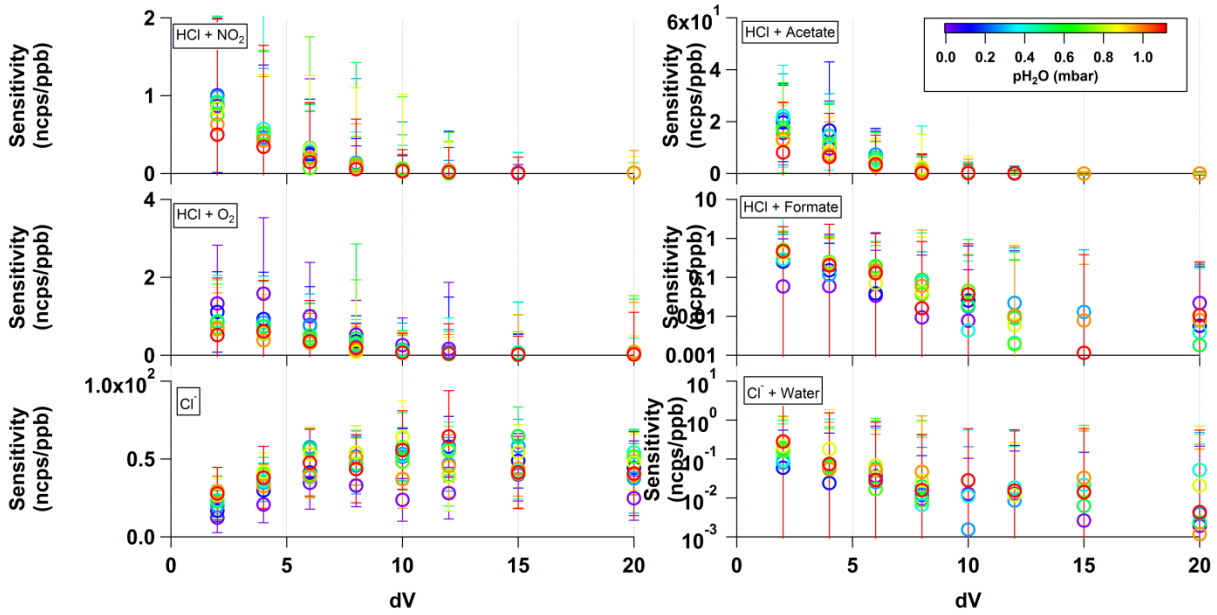

Figure SI10: The sensitivity to hydrochloric acid and related clusters is plotted against the voltage difference applied between the skimmer and BSQ front (component relation 5). The points are colored by the calculated partial pressure of water in the IMR corresponding to changing the relative humidity from 0% to 80% under laboratory conditions. Sensitivity drops off at higher dV values for clustered species but is maintained for declustered-deprotonated ions.

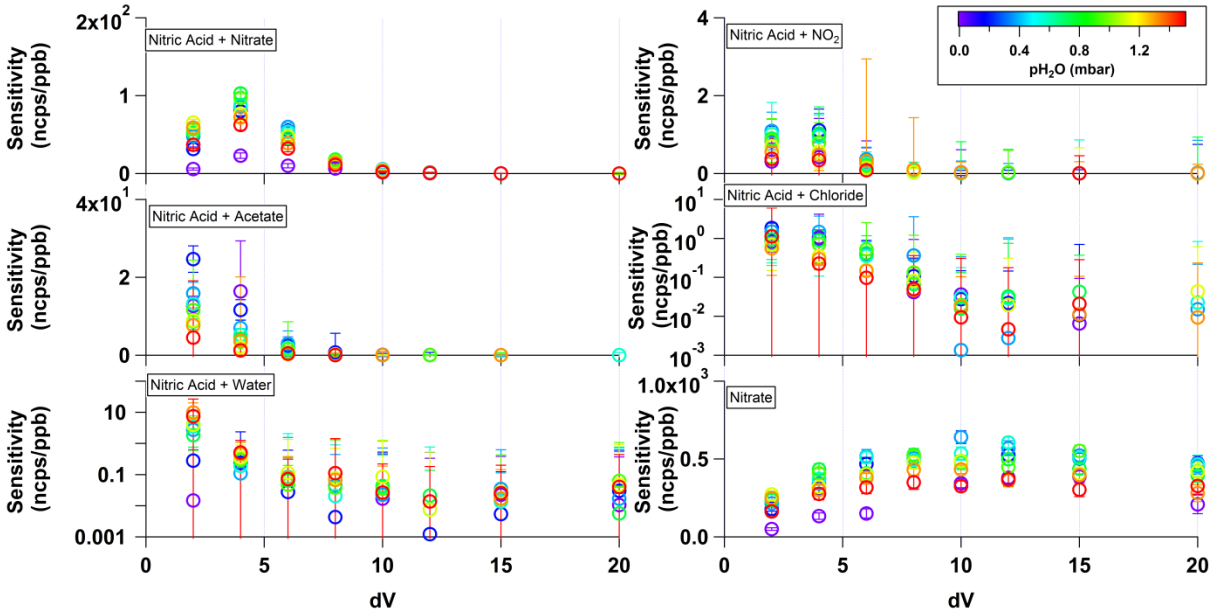

Figure SI11: The sensitivity to nitric acid and related clusters is plotted against the voltage difference applied between the skimmer and BSQ front (component relation 5). The points are colored by the calculated partial pressure of water in the IMR corresponding to changing the relative humidity from 0% to 80% under laboratory conditions. Sensitivity drops off at higher dV values for clustered species but is maintained for declustered-deprotonated ions.

SI 5.2 Sensitivity Ratios

$$\text{Sensitivity Ratio} = \frac{S_{RH,dV}[RC(O)OH+X]}{S_{RH,dV}(RC(O)O^-)} \qquad \text{(SI Eqn. 1)}$$

The sensitivity ratio is defined as the sensitivity at some relative humidity and voltage configuration ($S_{RH,dV}$) of some cluster [RC(O)OH+X] divided by the sensitivity at the same relative humidity and voltage configuration ($S_{RH,dV}$) of the deprotonated-declustered ion during the calibration [RC(O)O$^-$]. These plots (along with the LOD plots SI 4.3) show another way of examining how much a cluster can contribute to an observed signal relative to the signal of the identified deprotonated-declustered ion. It should be noted that if linear regression converges in the automated calibration curve processing script, it is included in this plot to provide an estimate of a calibration factor. At high dV values, many of the cluster calibration curves show poor r^2 values and the trend of decreasing sensitivity ratio as a function of dV will weaken.

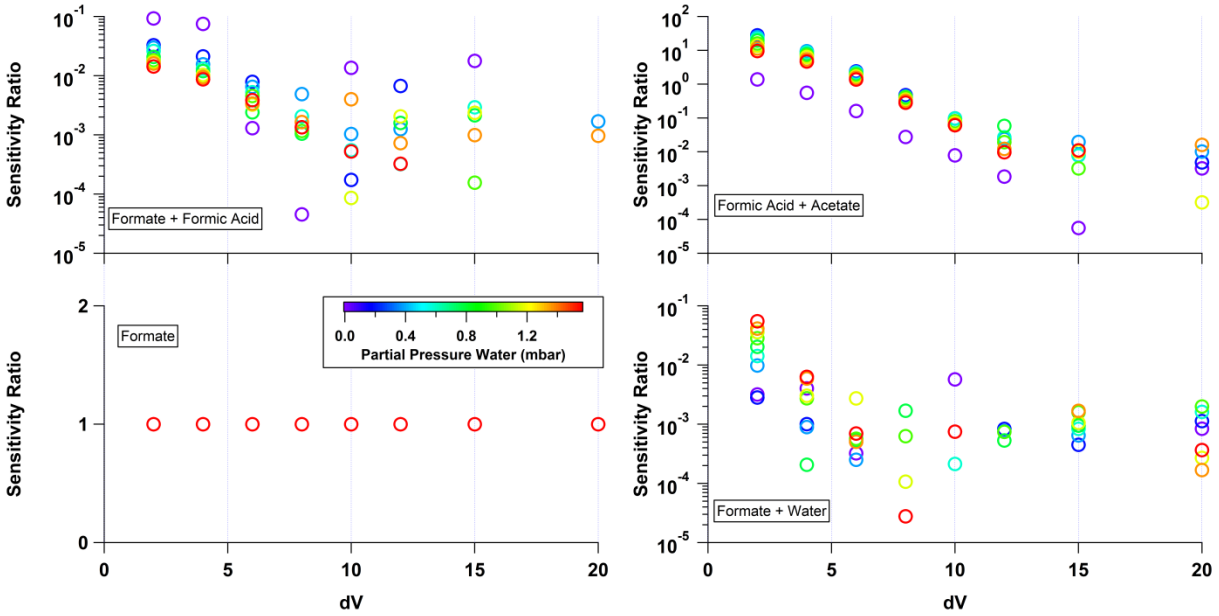

Figure SI12: Sensitivity ratios of various formic acid clusters relative to the sensitivity of formic acid under a variety of relative humidity conditions and voltage configurations. The contribution of the formic acid clusters to the observed mass spectrum decreases relative to the contribution at the deprotonated-declustered mass as dV increases.

.

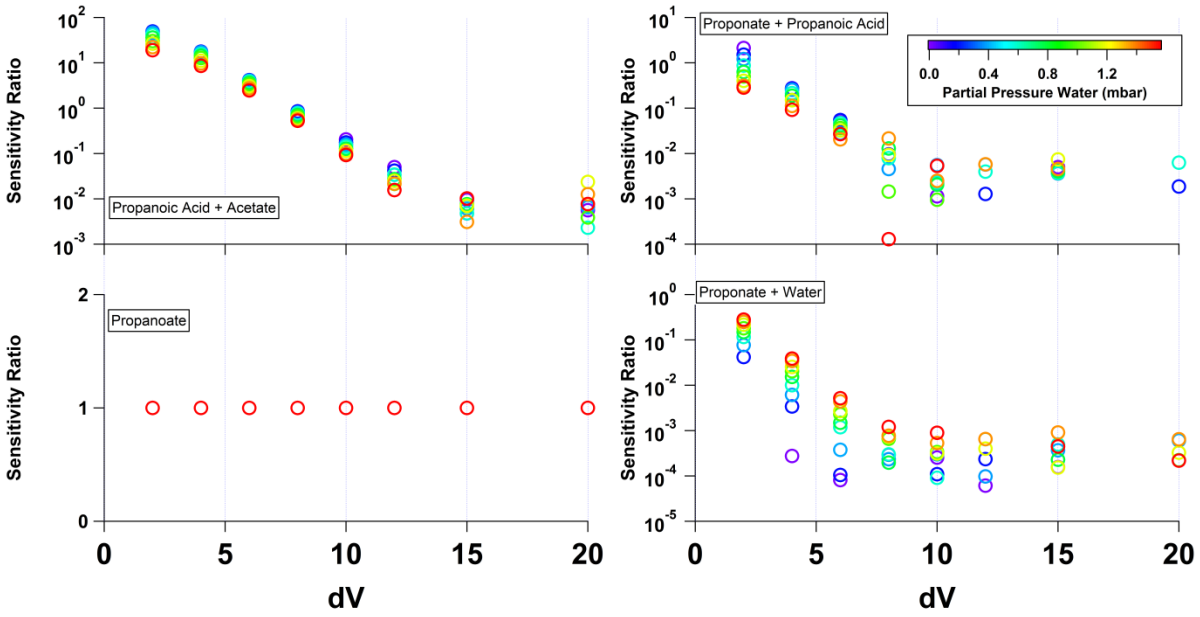

Figure SI13: Sensitivity ratios of various propanoic acid clusters relative to the sensitivity of propanoic acid under a variety of relative humidity conditions and voltage configurations. The contribution of the propanoic acid clusters to the observed mass spectrum decreases relative to the contribution at the deprotonated-declustered mass as dV increases.

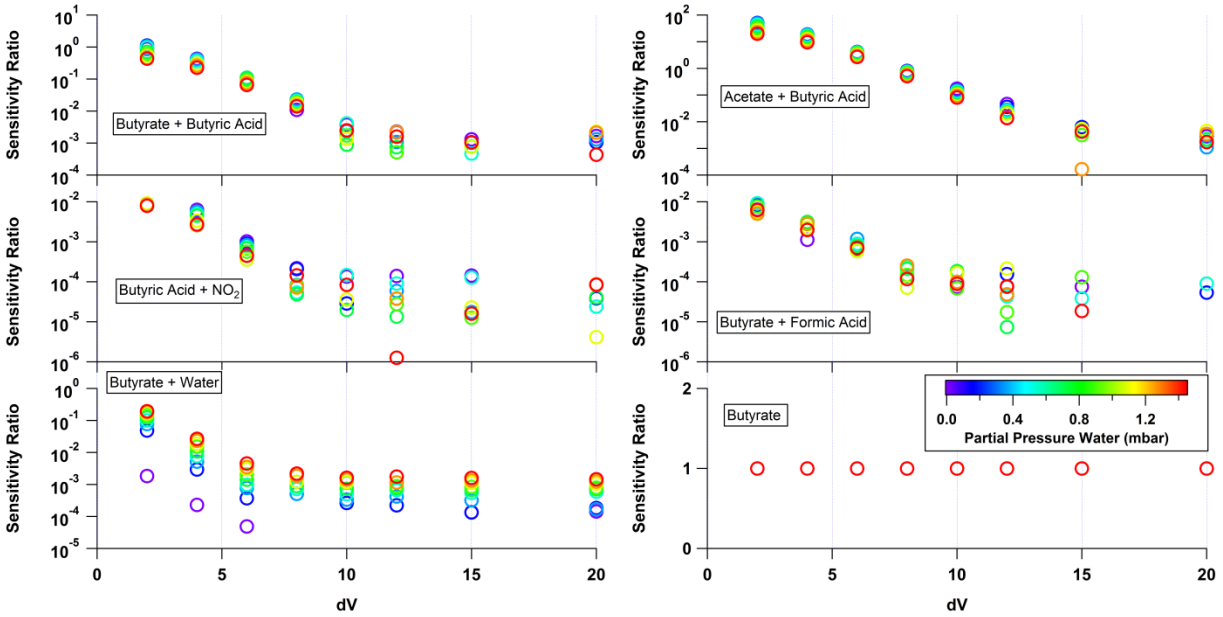

Figure SI14: Sensitivity ratios of various butyric acid clusters relative to the sensitivity of butyric acid under a variety of relative humidity conditions and voltage configurations. The contribution of the butyric acid clusters to the observed mass spectrum decreases relative to the contribution at the deprotonated-declustered mass as dV increases.

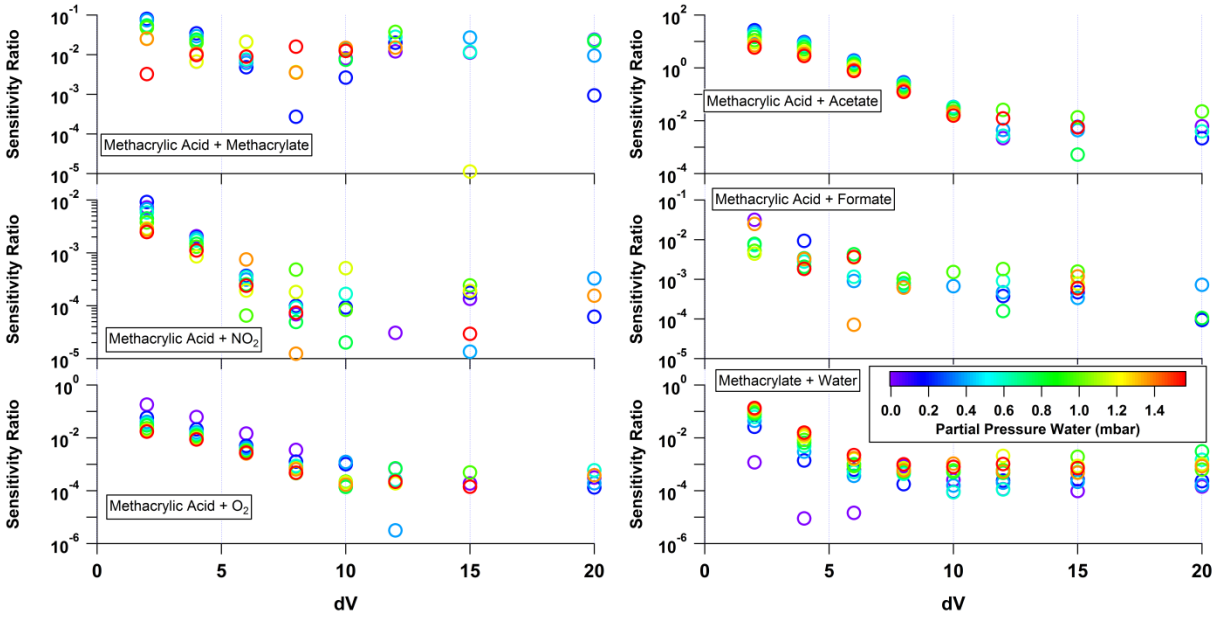

Figure SI15: Sensitivity ratios of various methacrylic acid clusters relative to the sensitivity of methacrylic acid under a variety of relative humidity conditions and voltage configurations. The contribution of the methacrylic acid clusters to the observed mass spectrum decreases relative to the contribution at the deprotonated-declustered mass as dV increases. Here, the deprotonated-declustered methacrylate ion is removed (it always equals 1), and the methacrylic acid self-cluster is included.

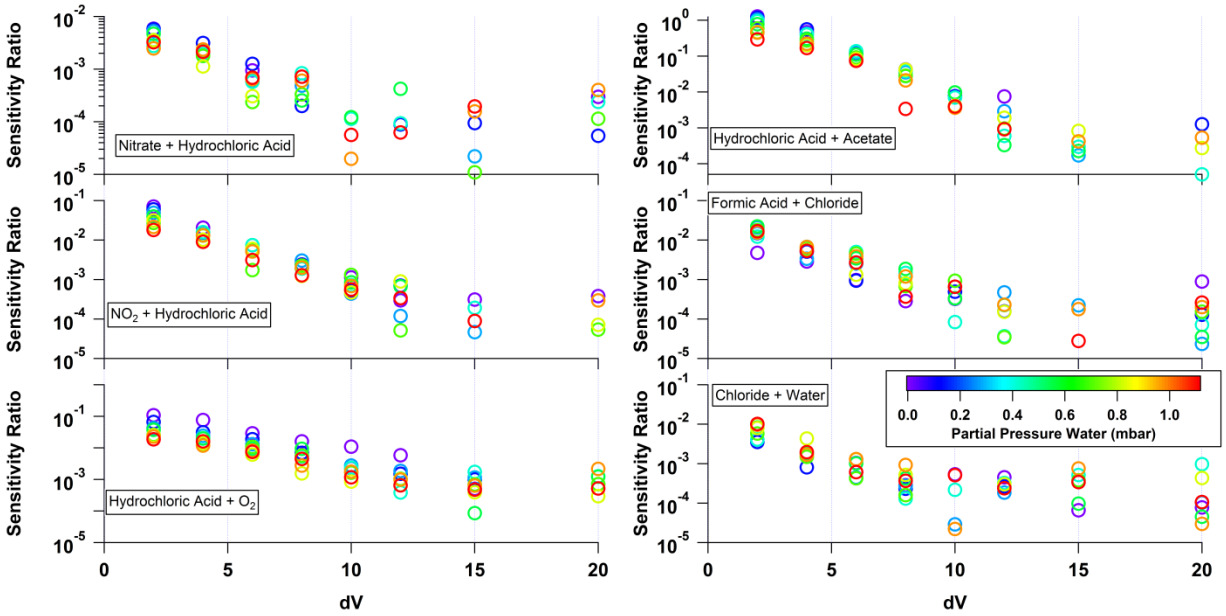

Figure SI16: Sensitivity ratios of various hydrochloric acid clusters relative to the sensitivity of hydrochloric acid under a variety of relative humidity conditions and voltage configurations. The contribution of the hydrochloric acid clusters to the observed mass spectrum decreases relative to the contribution at the deprotonated-declustered mass as dV increases. Here, the deprotonated-declustered chloride ion is removed (it always equals 1), and the [nitrate+hydrochloric acid] cluster is included.

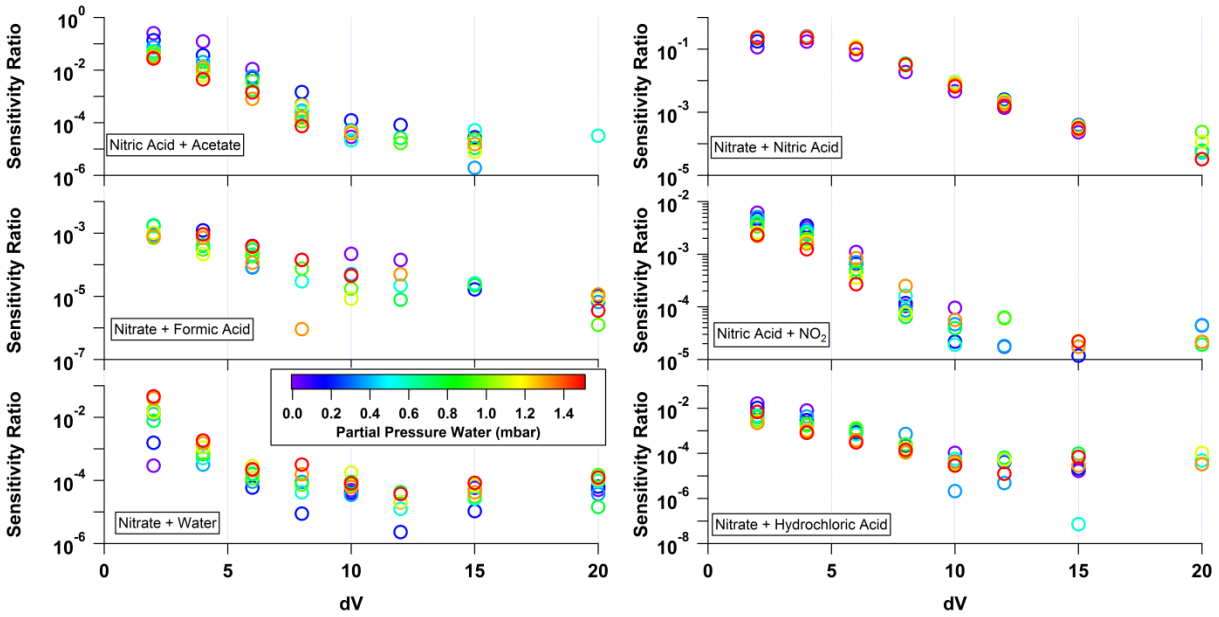

Figure SI17: Sensitivity ratios of various nitric acid clusters relative to the sensitivity of nitric acid under a variety of relative humidity conditions and voltage configurations. The contribution of the nitric acid clusters to the observed mass spectrum decreases relative to the contribution at the deprotonated-declustered mass as dV increases. Here, the deprotonated-declustered nitrate ion is removed (it always equals 1), and the [nitrate+formic] acid self-cluster is included.

SI 5.3 Limit of Detection

LOD: S/N=3

$$\frac{S}{N} = \frac{C_f[x]t}{\sqrt{C_f[x]t+2Bt}} \qquad \text{(SI Eqn. 2)}$$

The limit of detection (LOD) is calculated via SI Eqn. 2 following the work of Bertram *et al.* (2011) and application by Brophy and Farmer (2015). S/N is the signal-to-noise ratio, C_f is the calibration factor, [x] is the mixing ratio, t is the integration time, and B is the background count rate. This derivation assumes Poisson statistics. These plots show at what concentration clustering is going to contribute to the observed mass spectrum with statistical significance.

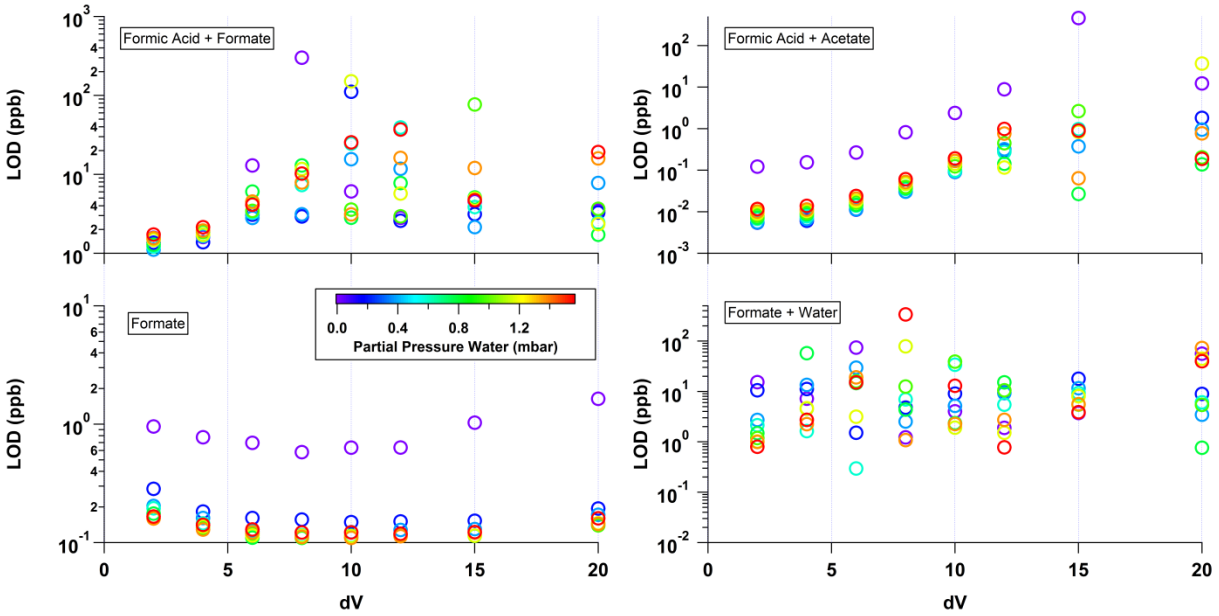

Figure SI18: The calculated 1 s (S/N=3) limit of detection of formic acid and related clusters is plotted against the voltage difference applied between the skimmer and BSQ front (component relation 5). The points are colored by the calculated partial pressure of water in the IMR corresponding to changing the relative humidity from 0% to 80% under laboratory conditions. The limit of detection is observed to increase or become sporadic at higher dV values for clusters while declustered-deprotonated species remain detectable at low concentrations.

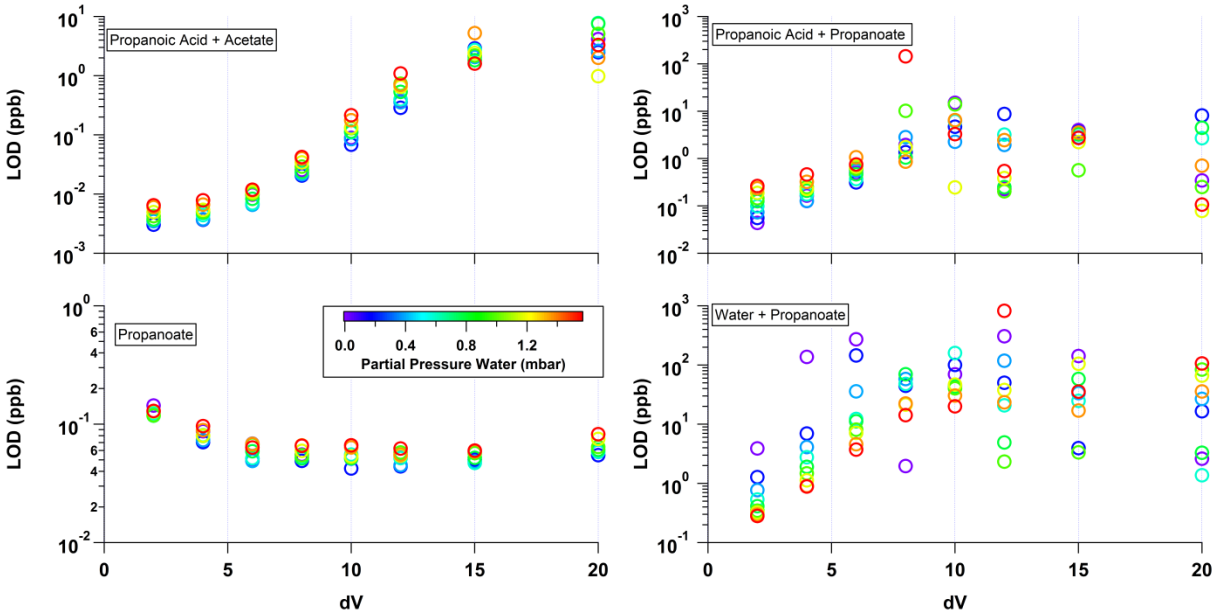

Figure SI19: The calculated 1 s (S/N=3) limit of detection of propanoic acid and related clusters is plotted against the voltage difference applied between the skimmer and BSQ front (component relation 5). The points are colored by the calculated partial pressure of water in the IMR corresponding to changing the relative humidity from 0% to 80% under laboratory conditions. The limit of detection is observed to increase or become sporadic at higher dV values for clusters while declustered-deprotonated species remain detectable at low concentrations.

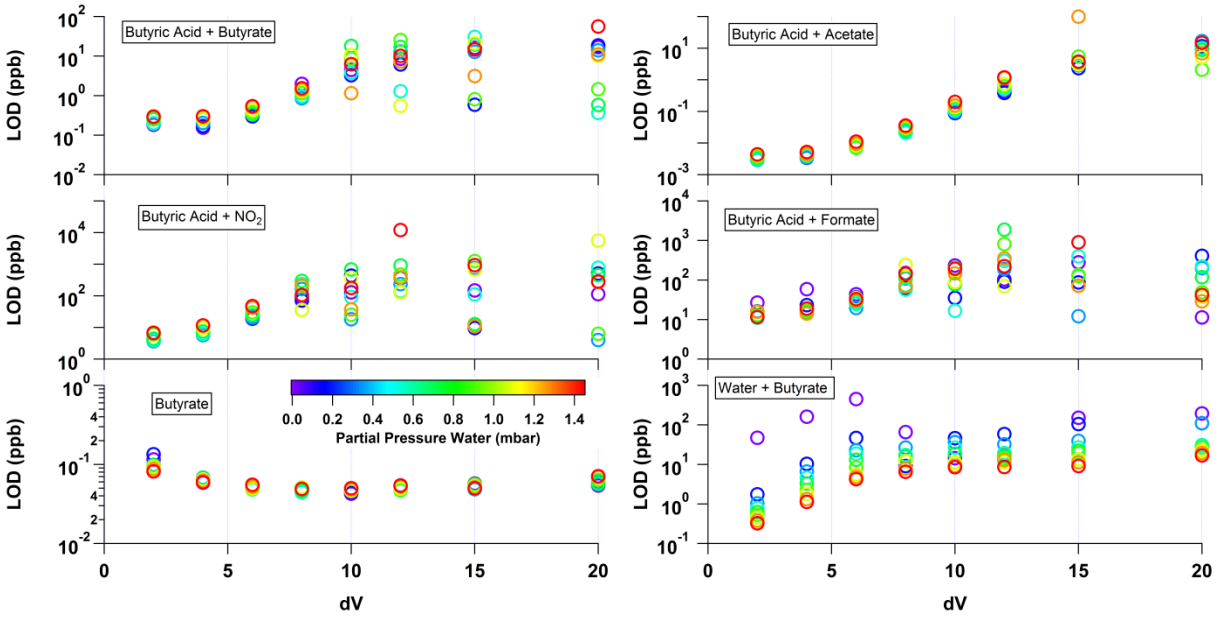

Figure SI20: The calculated 1 s (S/N=3) limit of detection of butyric acid and related clusters is plotted against the voltage difference applied between the skimmer and BSQ front (component relation 5). The points are colored by the calculated partial pressure of water in the IMR corresponding to changing the relative humidity from 0% to 80% under laboratory conditions. The limit of detection is observed to increase or become sporadic at higher dV values for clusters while declustered-deprotonated species remain detectable at low concentrations.

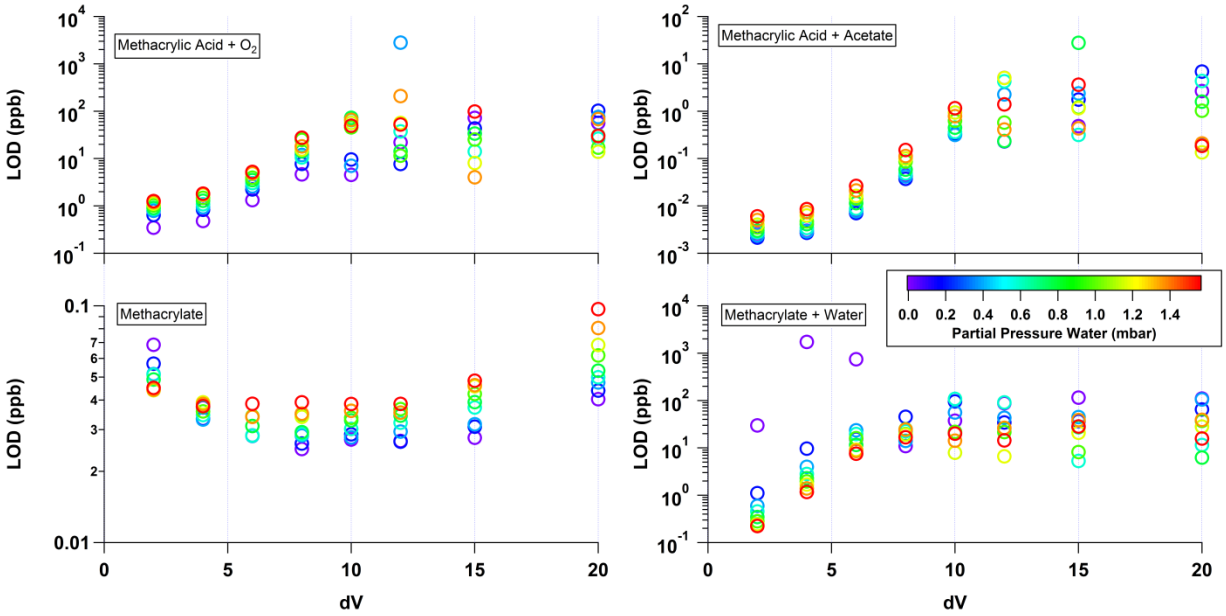

Figure SI21: The calculated 1 s (S/N=3) limit of detection of methacrylic acid and related clusters is plotted against the voltage difference applied between the skimmer and BSQ front (component relation 5). The points are colored by the calculated partial pressure of water in the IMR corresponding to changing the relative humidity from 0% to 80% under laboratory conditions. The limit of detection is observed to increase or become sporadic at higher dV values for clusters while declustered-deprotonated species remain detectable at low concentrations.

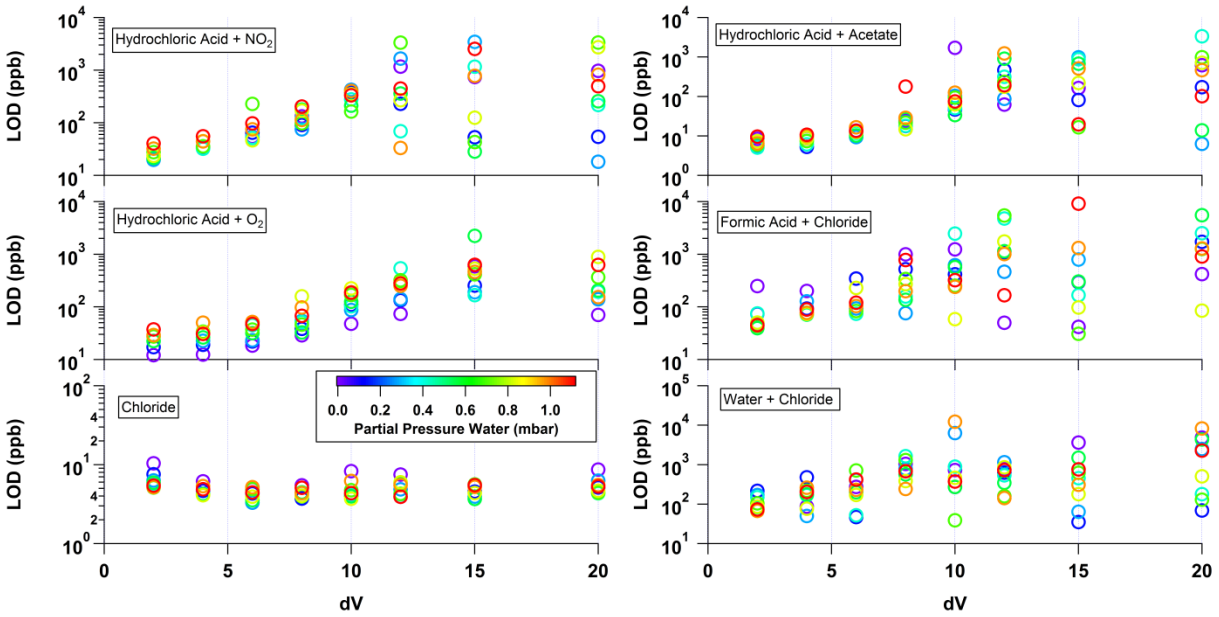

Figure SI22: The calculated 1 s (S/N=3) limit of detection of hydrochloric acid and related clusters is plotted against the voltage difference applied between the skimmer and BSQ front (component relation 5). The points are colored by the calculated partial pressure of water in the IMR corresponding to changing the relative humidity from 0% to 80% under laboratory conditions. The limit of detection is observed to increase or become sporadic at higher dV values for clusters while declustered-deprotonated species remain detectable at low concentrations.

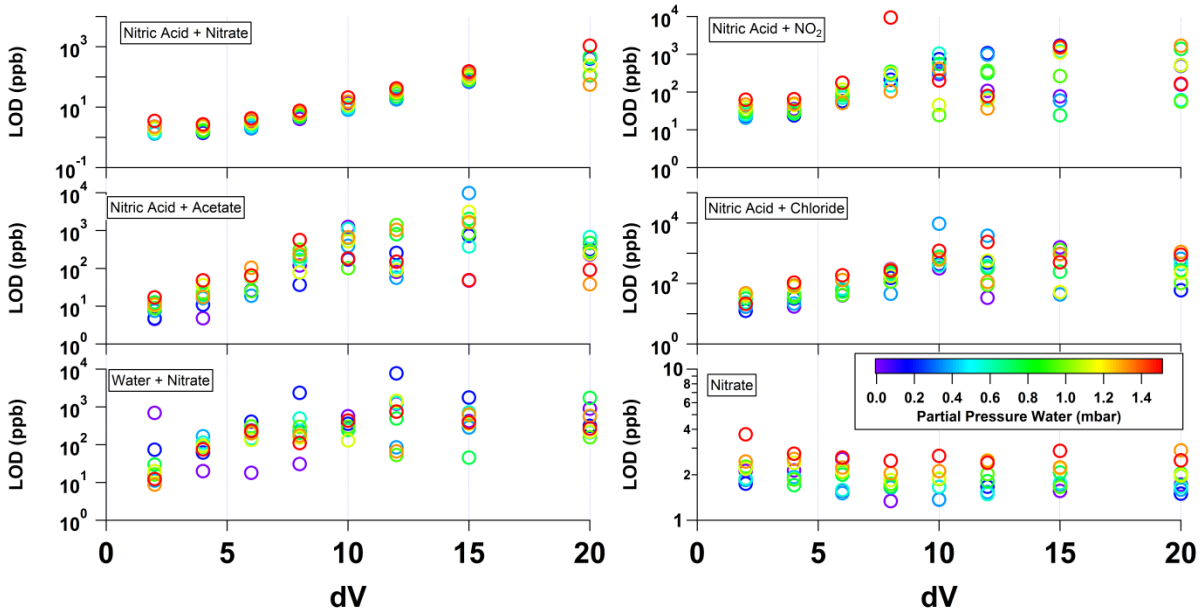

Figure SI23: The calculated 1 s (S/N=3) limit of detection of nitric acid and related clusters is plotted against the voltage difference applied between the skimmer and BSQ front (component relation 5). The points are colored by the calculated partial pressure of water in the IMR corresponding to changing the relative humidity from 0% to 80% under laboratory conditions. The limit of detection is observed to increase or become sporadic at higher dV values for clusters while declustered-deprotonated species remain detectable at low concentrations.

SI6: Evaluation of Chhabra Method for Dealing with Cluster Contributions

Chhabra et al. (2015) formulate the expression that the clustered mass intensity ($I_{i+acetate}$) is equal to the sum of the cluster ($I_{i'}$) plus a non-clustered ion with the same exact mass (I_j). Thus:

$$I_{i+acetate} = I_{i'} + I_j \qquad \text{(SI Eqn. 3)}$$

Next, the authors assume that the ratio between $I_{i'}$ and I_i is constant and no more than the acetate ratio of 0.2 in their study. Either the $I_{i+acetate}$ to I_i ratio, or 0.2 is used (whichever value is smaller) to determine the contribution of the clustered species to the mass $I_{i+acetate}$.

$$I_{i'} \approx (I_{i+acetate}/I_i) \times I_j \quad \text{OR} \quad I_{i'} \approx 0.2 \times I_j \qquad \text{(SI Eqn. 4)}$$

An acetate ratio of 0.2 in our system corresponds to operating component relation 5 at a dV of ~6 V (actual acetate ratio of 0.16). Here, the relative contribution of propionic acid to the [propionic acid + acetate]$^-$ cluster ranges between 2.47 and 4.15 depending on the relative humidity. The relative contribution of formic acid to the [formic acid + acetate]$^-$ cluster ranges between 0.16 to 2.38. The relative contribution of butyric acid to the [butyric acid + acetate]$^-$ cluster ranges between 2.67 and 4.1. The relative contribution of methacrylic acid to the [methacrylic acid + acetate]$^-$ cluster ranges between 0.77 and 1.89. The self-cluster of propionic acid contributes only 0.054 and the water-cluster contributes an order of magnitude less relative to the deprotonated-declustered sensitivity. This is a consistent story for all the alkanoic acids evaluated. Nitric acid provides an interesting example. The [nitric acid + acetate]$^-$ cluster contributes between 0.011 and 0.008 relative to the nitrate signal while the nitric acid self-cluster contributes between 0.12 and 0.06 relative to nitrate. This self-cluster is not addressed by these recommendations.